Ocean Engineering 253 (2022) 111290

Contents lists available at ScienceDirect

Ocean Engineering

journal homepage: www.elsevier.com/locate/oceaneng

Shock effects of underwater explosion on naval ship foundations: Validation of numerical models by dedicated tests

F. Mannacio [a,b,*], A. Barbato [c], F. Di Marzo [a], M. Gaiotti [b], C.M. Rizzo [b], M. Venturini [a]

[a] Italian Navy, Naval Experimentation and Support Centre, CSSN, Viale S. Bartolomeo, 400, 19126, La Spezia, Italy
[b] University of Genova, Polytechnic School, DITEN, via Montallegro, 1, 16145, Genova, Italy
[c] Fincantieri Naval Vessel Business Unit, Via Cipro, 11, 16129, Genova, Italy

ARTICLE INFO

Keywords:
Underwater explosion
Numerical
Experimental
Shock
Foundation

ABSTRACT

The underwater shock explosions can cause severe damage not only to the naval ships machinery and equipment, but also to their foundation structures, that are a critical part of the system integration. A few national rules allow shock resistance verification by means of dedicated calculations as it is in general not possible the testing of the complete system machine-foundation. Dynamic structural analysis of foundations by Finite Element Method (FEM) is accepted, but no detailed modelling strategies, procedures and inputs are provided. The aim of this paper is to provide some reliable guidelines of shock foundation design, comparing the results obtained by the numerical simulation with the experimental data collected performing a series of dedicated shock tests carried out according to the MIL S 901 D medium weight shock standard. Eventually, it is shown that experimental and numerical analyses performed in parallel may support each other to provide better understanding of complex phenomena.

1. Introduction and motivation of the work

Shock underwater explosions result into severe loads not only for equipment, but also for their foundations, especially when they are rigidly connected and the machinery has small mass as reported in SMM/CN 300 DVD (1978). In the military common practice, the machinery is shock tested, according to MIL S 901 D (1989) standards, while the relevant foundations are normally verified by calculation. In early design phases, in fact, it is in general not possible the testing of the equipment including the relevant structural foundations, then a verification criterion must be assessed for the foundations relevant to shock tested equipment. Rules allow scantling assessment with static, statistic Shock Response Spectrum methods or transient dynamic calculations, through a displacement time history to be applied at the basis of the structure. The Dynamic Design Analysis Method (DDAM), as described in NAVSEA 0908-LP-000-3010 Rev. 1 (1995), is a widely recognized method in naval engineering practice (Remmers et al., 1996; Scavuzzo and Pusey, 2002). However, national shock requirements are not always based on Shock Response Spectrum based on NRL-Coefficients, as that used in DDAM and reported in the work of O'Hara and Belsheim (1963). Often, analysis in time domain and experiments are necessary. Therefore, the shock designer can use a Shock Response Spectrum method, if allowed by rules and Customer specifications, or a dynamic transient method, which is more complex but more generally applicable, starting from a displacement, velocity or acceleration time history. This last choice, in particular, can cope with non-linear problems (being an analysis in frequency domain implicitly linear) and it is particularly useful to analyse equipment and related foundation on non-linear mountings and to obtain directly the simulated behaviour of the structure. In any case, no detailed modelling strategies, procedures and inputs have been provided in literature, hence the need of research. The aim of the work is to provide some reliable guidelines useful in the design phase to perform a dynamic calculation: the validation of the model is checked comparing the numerical results with data achieved from tests, properly designed for the purpose, carried out according to the MIL S 901 D medium weight shock standard.

NAV 30 A001 (1986), MIL S 901 D (1989) and STANAG 4141 (1976) provide guidance about the shock resistance verification of machinery and equipment by means of the Medium Weight Shock Machine currently adopted by Italian Navy: in this case, typical structural foundations are replaced by standard mounting fixtures. In NAVSEA 0908-LP-000-3010 (1995) the Dynamic Design Analysis Method

* Corresponding author. Italian Navy, Naval Experimentation and Support Centre, CSSN, Viale S. Bartolomeo, 400, 19126, La Spezia, Italy.
E-mail addresses: francesco.mannacio@marina.difesa.it (F. Mannacio), alfonso.barbato@fincantieri.it (A. Barbato), fabrizio_dimarzo@marina.difesa.it (F. Di Marzo), marco.gaiotti@unige.it (M. Gaiotti), cesare.rizzo@unige.it (C.M. Rizzo), marco_venturini@marina.difesa.it (M. Venturini).

https://doi.org/10.1016/j.oceaneng.2022.111290
Received 13 October 2021; Received in revised form 9 March 2022; Accepted 8 April 2022
Available online 5 May 2022
0029-8018/© 2022 Elsevier Ltd. All rights reserved.

(DDAM) is presented and it is accepted for sizing a foundation structure. In the work of Coats et al. (2003) some guidelines are given for the system being modelled, in compliance with NAVSEA (1995). Italian SMM/CN 300 DVD (1978) rule allows verification analysis for foundation structures by calculation, without getting into numerical simulation details. In this paper, dedicated shock tests are carried out onto a typical foundation structure and measurements are compared with Finite Element (FE) results obtained by non-linear dynamic implicit calculation (Mannacio et al., 2021) with the purpose of validating the FE proposed procedure.

At first, experimental and numerical modal analysis are performed in parallel to estimate natural frequencies and to define an adequate time step for further dynamic calculations. Then, implicit dynamic calculations, according to Bathe Method (ADINA, 2015; Bathe, 2014), are run, imposing as dynamic load input the displacement time histories experimentally measured by means of accelerometers at the base of the structure, and considering only gravity as static load input. Calculations and experimental shock tests are carried out considering both rigid connections and elastic mountings, modelled with connector elements simulating their stiffness and damping. In the FE simulation three different models of mounting are proposed to evaluate their accuracy with reference to the experimental results. The validation of the calculation method is checked comparing its results with test data achieved using the high-impact shock machine for medium weight. The results of the comparison are presented for both the rigid and the elastic case.

2. Experimental analysis

2.1. Test set-up

The experimental analysis consists in testing a foundation structure made by two 275 JR steel parallel UPN 100 beams, 1.2 m long. A 250 kg mass is used to simulate the weight of the machinery. In the first series of tests the mass is directly bolted to the foundation beams; in the second, instead, it is connected to these beams by mountings, type POWERFLEX PWHS0953008 (POWERFLEX, 2010).

Experimental modal analysis (EMA) (Ewins, 2000) was carried out suspending the structure on four rubber bands, see Fig. 1. The hammer-roving method is used, which consists in hammering three times (in order to get a mean value of Frequency Response Function – FRF) in the three directions X, Y and Z (longitudinal, transversal and vertical) with an instrumented hammer in a single reference point (no. 45 in Fig. 2) and in moving a triaxial accelerometer for each test in 44 different points (see Fig. 3). The sampling frequency is 1000 Hz which is more than adequate for this work interest band of analysis that is from 0 to 450 Hz.

The nine FRFs functions measured in each point are analyzed using the Me Scope ME'scope VES (2014) commercial software to obtain natural frequencies, damping and modal participation factors. The number of peaks for each function is counted using the Multi-Reference CMIFs (Complex Mode Indicator Functions) algorithm in the Me Scope

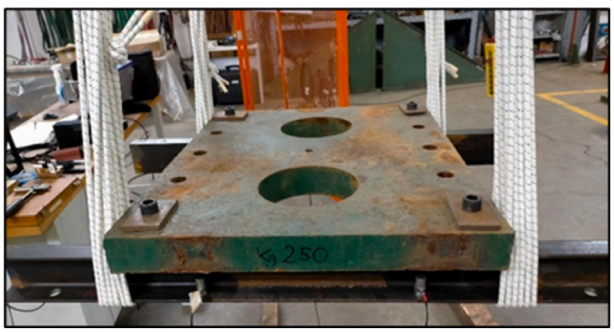

Fig. 1. Experimental modal analysis structure.

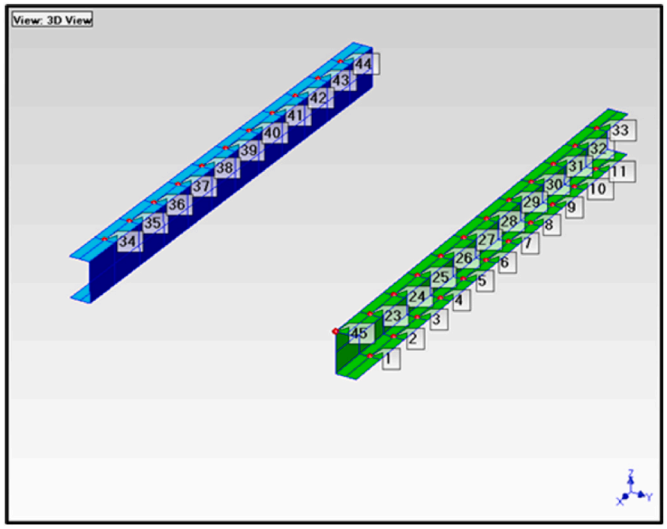

Fig. 2. Experimental modal analysis: measurement point scheme.

Fig. 3. Experimental modal analysis: vertical hammer and accelerometers in point no. 1.

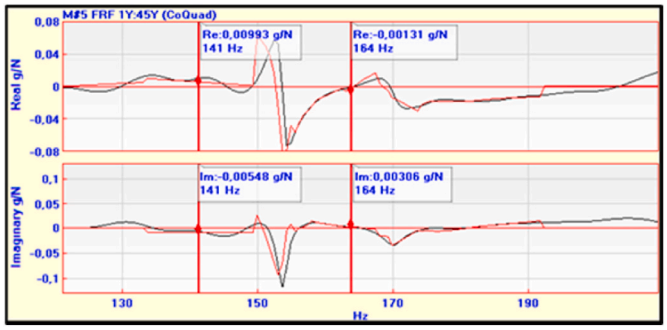

Fig. 4. Example of measured (black) and curve fitted (red) FRF close to 152 Hz. (For interpretation of the references to colour in this figure legend, the reader is referred to the Web version of this article.)

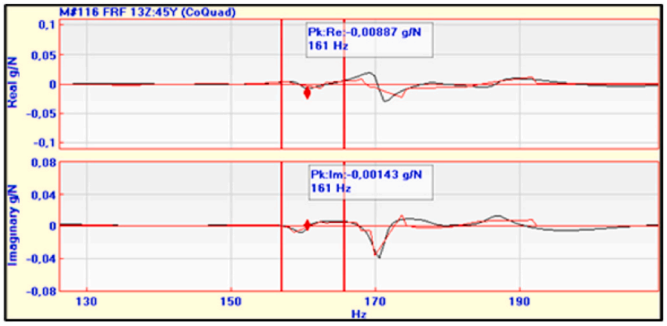

Fig. 5. Example of measured (black) and curve fitted (red) FRF close to 161 Hz. (For interpretation of the references to colour in this figure legend, the reader is referred to the Web version of this article.)

Select Mode	Frequency Hz	Participation	Damping (%)	Damping Hz
1	152	(0,16,0,98,-0,03)	0,893	1,36
2	161	(-0,09,0,12,-0,98)	0,814	1,31
3	174	(0,97,0,00,-0,22)	0,608	1,06
4	283	(0,96,-0,09,0,00)	0,387	1,09
5	314	(0,03,-0,91,-0,13)	0,369	1,16
6	366	(-0,97,0,02,0,13)	0,464	1,7

Fig. 6. Experimental natural frequencies, damping and modal participation factor in the three directions (X, Y and Z).

Ves environment. The curve fitting function for the determination of the natural frequencies and related Eigenvalues is carried out using the Multi-Reference Quick Fit method. Figs. 4–5 show examples of FRFs: the black curve is the signal measured, the red curve, instead, is that reconstructed by the software through curve fitting algorithm. Fig. 6 shows natural frequencies, damping (in percentage and half power band as well) and modal participation factors in the three directions, X, Y and Z.

The modal analysis was deemed necessary both to validate the analysis model and to define an adequate shock test set-up.

2.2. Rigid shock test setting and testing

For the shock tests a MIL S 901 D (1989) medium weight shock machine (MWSM), described in its theoretical behaviour by Clements (1972), is used, connecting the structure under test to the machine anvil table by means of standard mounting platforms. Accelerometers are set on the supporting channels to obtain the displacement time history at the foundation basis. The weight reference (350 kg) is chosen according

Fig. 7. Rigid shock test: accelerometers setting. Accelerometers on supporting channels are circled.

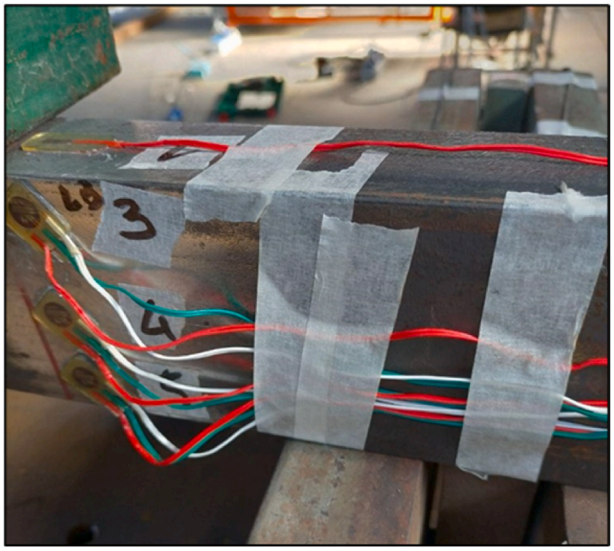

Fig. 8. Rigid shock test: strain gauges no. 1 (on top faceplate), 3, 4 and 5 (on web) set up.

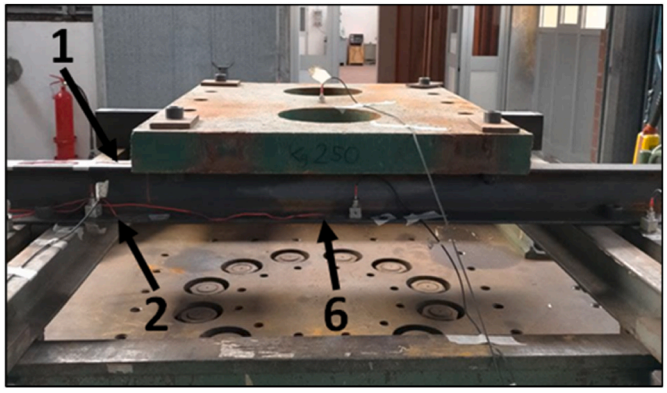

Fig. 9. Rigid shock test: strain gauges no. 1 (on top faceplate), 2 and 6 (on bottom faceplate) set up.

Table 1
Rigid shock test schedule for medium weight shock machine.

Test #	Hammer height	Anvil table travel
	m	m
1	0.300	0.076
2	0.300	0.076
3	0.300	0.076
4	0.300	0.076
5	0.600	0.076
6	0.600	0.038
7	0.600	0.076
8	0.600	0.038

to the MIL S 901 D (1989) rule criteria. In this value, it is considered the sum of the 250 kg of mass, the foundation beams and the standard mounting fixture weight. Shock loadings are produced in the vertical direction, varying the anvil table travel and the height of hammer drop. The structural response is measured by means of six strain gauges (no. 1-2-6 uniaxial and no. 3-4-5 triaxial rosette), that are bonded onto the foundation beams, close to the rigid connection of the mass. The sampling frequency of all measurements is 50 kHz. See Fig.s 7-9.

Eight vertical shock tests were carried out, increasing gradually the height of the drop hammer and varying the anvil table travel, as shown

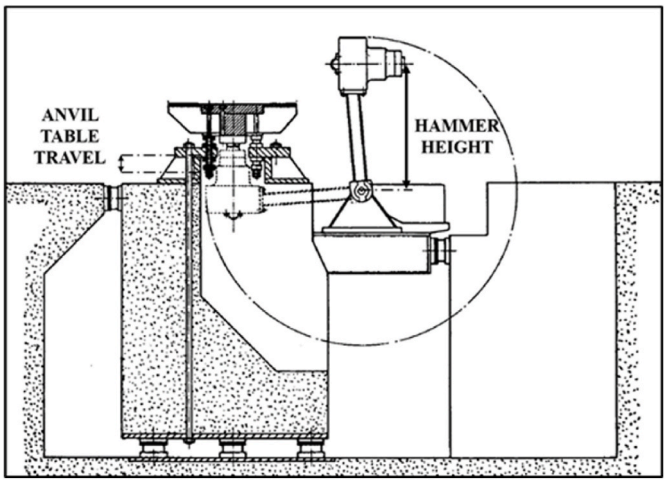

Fig. 10. MIL S 901 D medium weight shock machine scheme.

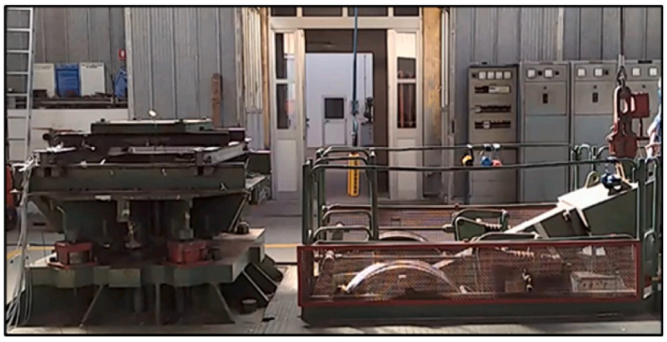

Fig. 11. Rigid shock test drop positioning.

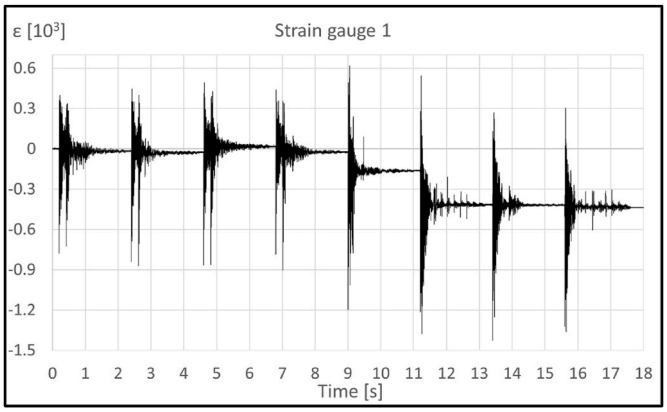

Fig. 12. Strain gauges no. 1 (top faceplate): longitudinal strain measurement sequence.

in Table 1 and Figs. 10–11.

The signals measured on the top faceplate (strain gauges no. 1) and on the top web (strain gauges no. 3) show the increase up to yielding from test no. 5 and onwards when the hammer height increases up to 60 cm (see Figs. 12–13).

The Fast Fourier Transform (FFT) diagrams made by strain gauges measurements confirm the EMA results showing the natural frequency in the vertical direction at 169 Hz, even if this has less energy during a shock impact and it tends to lose in the background noise (Fig. 14). Moreover, this frequency analysis shows that during the shock test other operational frequencies are observed at 59 Hz and 127 Hz, that exist

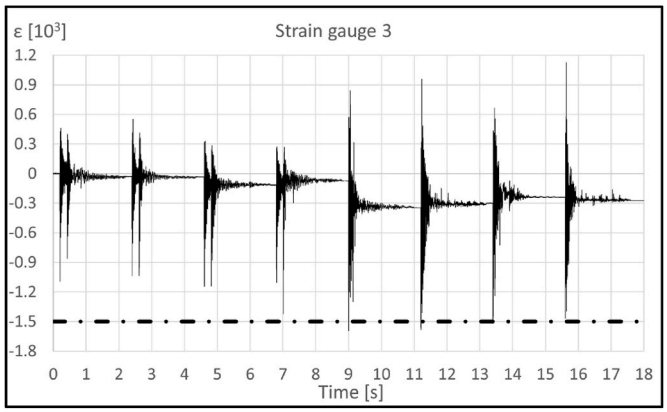

Fig. 13. Strain gauges no. 3 (top web): longitudinal strain measurement sequence. The dashed line represents the static yield threshold.

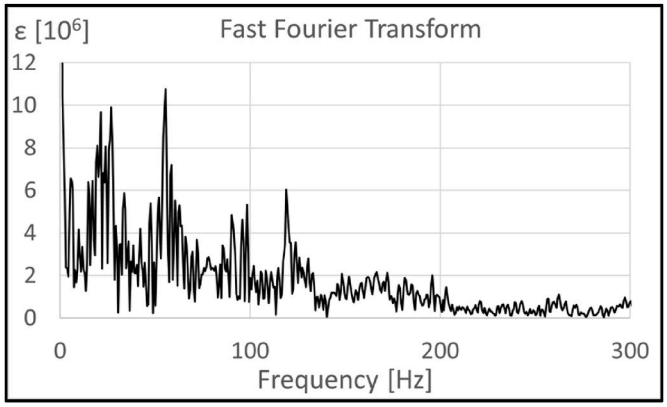

Fig. 14. Example of FFT diagram made by Strain gauge no. 3 measurements in Test no. 4.

only in connection with shock condition, but are not identified by EMA. These natural frequencies are caused by the frequency of installation support. In particular, 59 Hz is the natural frequency of the medium weight shock machine, as it is reported in the work of Clements (1972) .

2.3. Elastic shock test setting and testing

The shock test set-up is the same of the previous series of tests, but in this case the structure has been mounted on shock machine complete with elastic mountings (n° 4 antishock and antivibration stainless steel

Fig. 15. Shock test with mountings set up.

Fig. 16. Shock test with mountings: effects immediately after the drop hammer (image taken from recorded video).

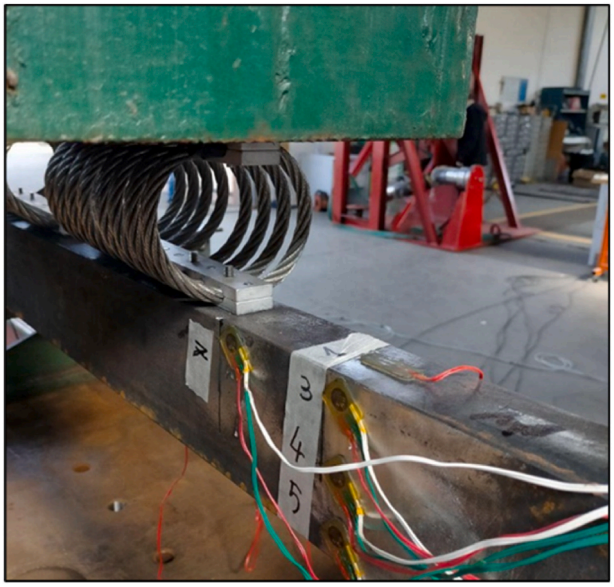

Fig. 17. Shock test with mountings: strain gauges no. 1 (top faceplate), 3, 4, 5 and 7 (web) set up.

Table 2
Shock test with mountings schedule for medium weight shock machine.

Test #	Hammer height	Anvil table travel
	m	m
1	0.200	0.076
2	0.300	0.076
3	0.600	0.076

cable dampers of company Powerflex model number "PWHS0953008") (see Figs. 15-16). In addition, a triaxial rosette strain gauge (no. 7) on web top is added to study the response close to the elastic connection (see Fig. 17). The foundation beams that were yielded in the rigid shock test are of course replaced.

No. 3 vertical shock tests are carried out, increasing gradually the height of the drop hammer (Table 2). In this case signals do not show plastic strain residual after the series of tests (see Figs. 18–19).

3. Numerical simulation

3.1. Finite element method model

The numerical analysis was performed using ADINA (2015) software. Two different models were built, the former considering a rigid connection, while the latter includes to modelling of an elastic support.

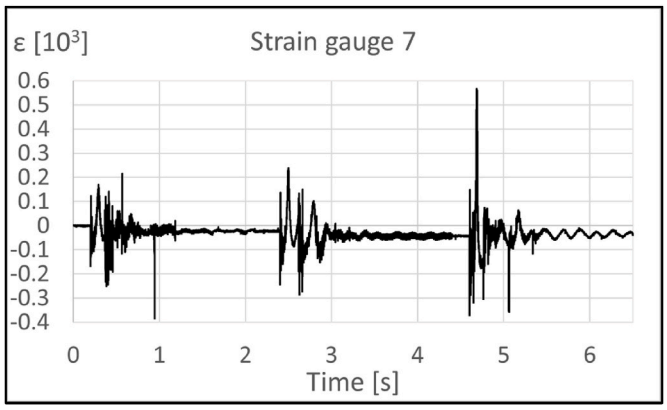

Fig. 18. Strain gauges no. 7 (top web): longitudinal strain measurement sequence.

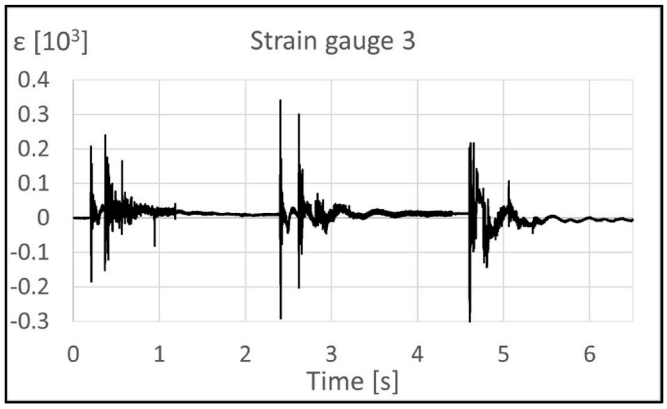

Fig. 19. Strain gauges no. 3 (top web): longitudinal strain measurement sequence.

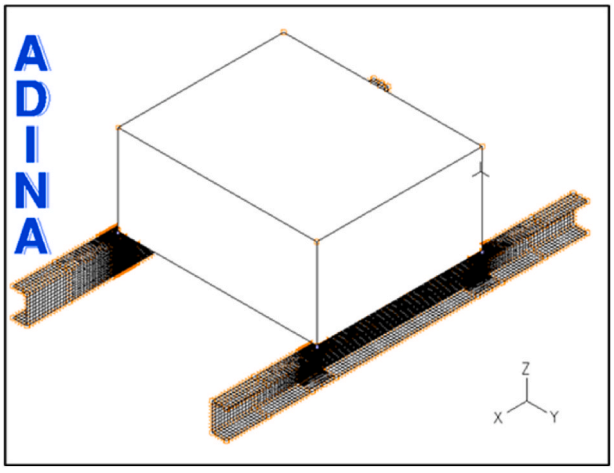

Fig. 20. Finite element model: rigid connection case.

In the FE environment the foundation is discretize into 4-nodes shell elements, while the mass is modelled using a 27-nodes volumetric element, with proper density properties (see Fig. 20). The mass is supposed to be more rigid than the foundation beams, so the elastic modulus of the relevant volumetric element is imposed suitably higher ($2.07{\cdot}10^{12}$ N/m^2) than the one of steel beams ($2.07{\cdot}10^{11}$ N/m^2).

The dynamic behaviour of the foundations material (steel 275 JR) is characterized extrapolating from the HIPEBA (2015) report the proper

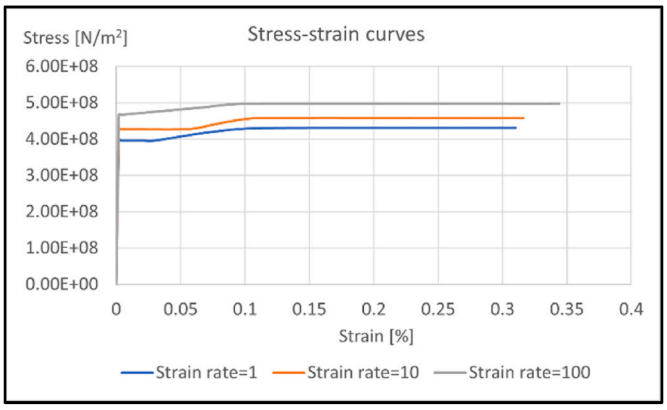

Fig. 21. Stress-strain curves (engineering stress) depending by strain rate (see HIPEBA (2015)).

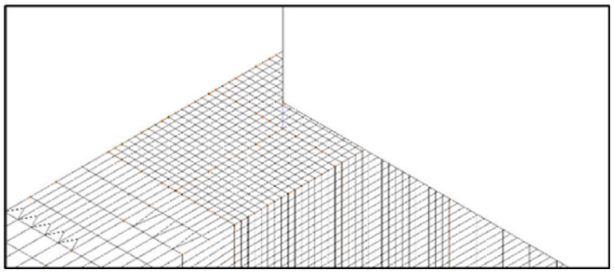

Fig. 22. Finite element method mesh close to the rigid connection.

stress-strain curves that depend on their strain rate function (see Fig. 21). The foundation is linked to the mass by means of rigid links (Coats et al., 2003) in the bolted case and connector elements with proper stiffness and damping in the elastic condition. Numerical drilling stiffness problems in the 6 DOF connection nodes of rigid links and connectors to neighbouring shell nodes are solved, using soft beam elements. This kind of constraint is linked to a single node, so that the stress concentration is relevant. To get around this issue, a 0.5 mm square area of elastic shell elements is modelled around the rigid links connection nodes.

A sensitivity analysis on mesh refinement has been carried out. Results in good agreement with experimental data are obtained selecting for the FEM model a very fine mesh patterns as that suggested by classification societies' rules for the two-dimensional elements FEM models (i.e. shell elements). Therefore, the shell elements mesh is chosen considering a relatively small length (2.5 mm) for the rectangular zone (80 mm longitudinally long) of the top faceplate and of the web close to the rigid or elastic connections (Fig. 22). The remaining part of the foundation is modelled by a coarser mesh (10 mm element size).

Mountings are modelled using connectors with stiffness properties defined by the non-linear symmetric curves load-displacement for compression/tension, shear and roll degrees of freedom (Fig. 23) and concentrated dampers with constant damping value (10%). The curves load-displacement and the damping value have been provided by mountings suppliers. Three different mounting models are proposed: the first consists of a single connector foundation-mass, the second of eight connectors set along a row and the third of 24 connectors distributed in a matrix (Fig. 24). In these two last models, the stiffness properties of each connector of a single mounting are evaluated considering that they are distributed in parallel. Moreover, the connectors are linked to the equipment using rigid links.

3.2. Modal analysis

A modal analysis using Enriched Subspace Iteration Method (ADINA, 2015; Bathe, 2014) is performed, starting from the solution of the static problem, where only gravity as mass proportional load is applied on the model. Simple supports are used as boundary condition to simulate the structure suspended on four rubber bands (Fig. 25). Natural frequencies and percentage masses are reported in Table 3. More of the 80%, according to NAVSEA 0908-LP-000-3010 (1995), of the percentage masses is in the range from 0 to 450 Hz (92% only in the vertical direction Z): this confirms the validity of the choice to carry out the Experimental Modal Analysis in this band.

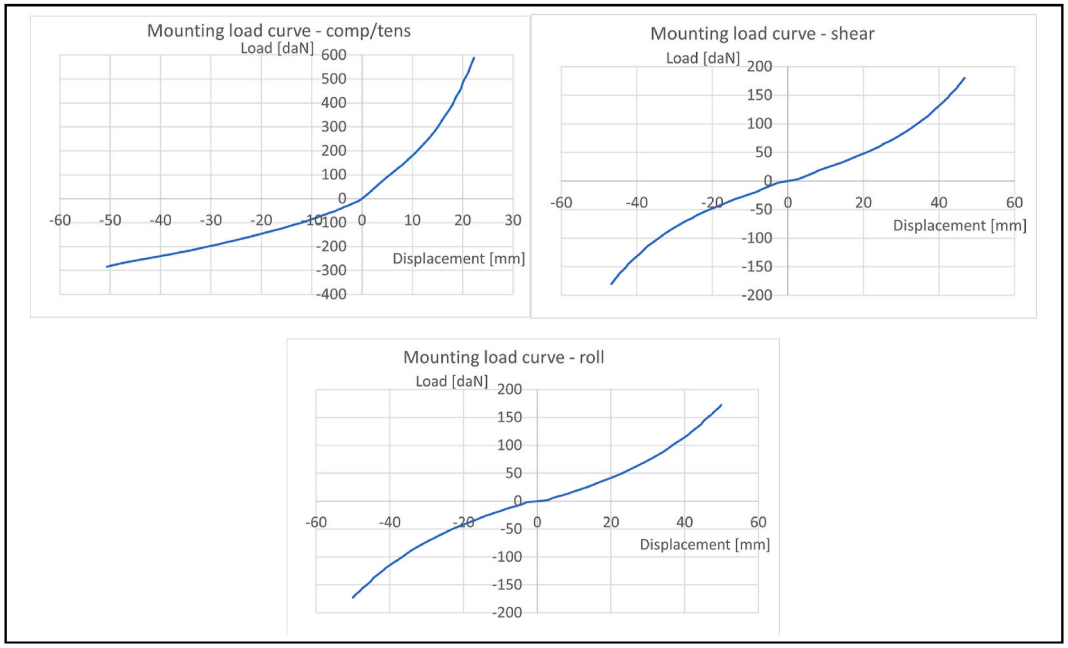

Fig. 23. Mounting loads curves provided by mounting suppliers – Compression/tension, shear and roll.

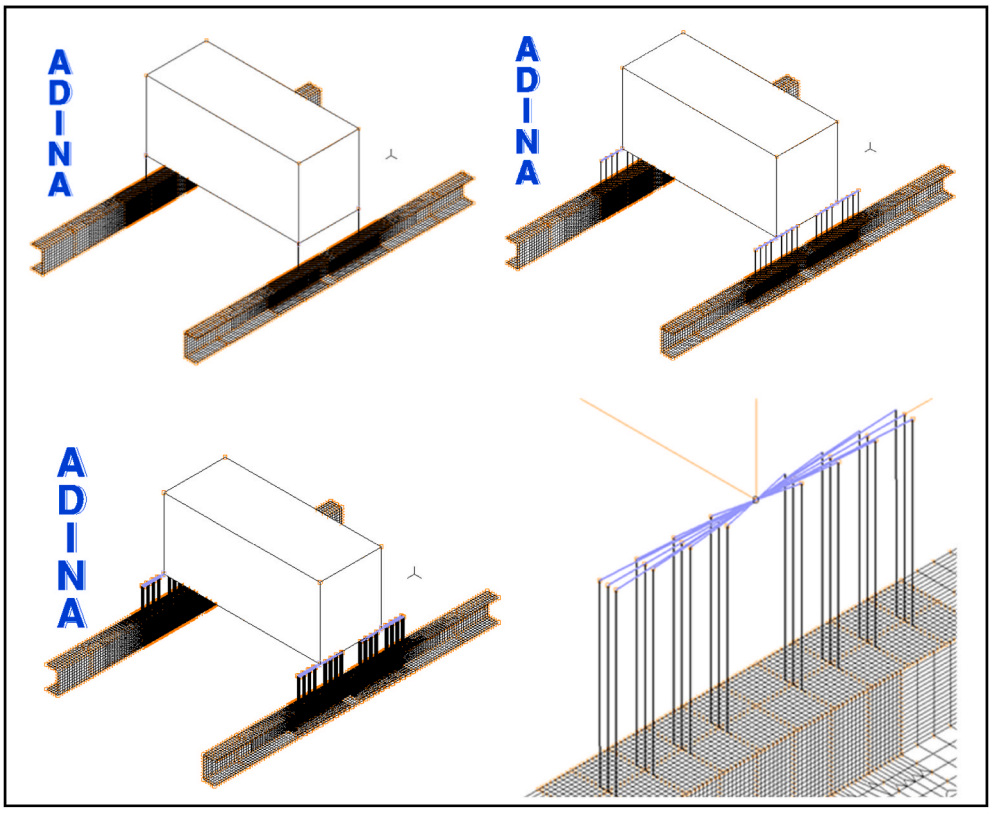

Fig. 24. FEM mounting models with 1, 8 and 24 connectors (a particular of 24 connectors model is shown).

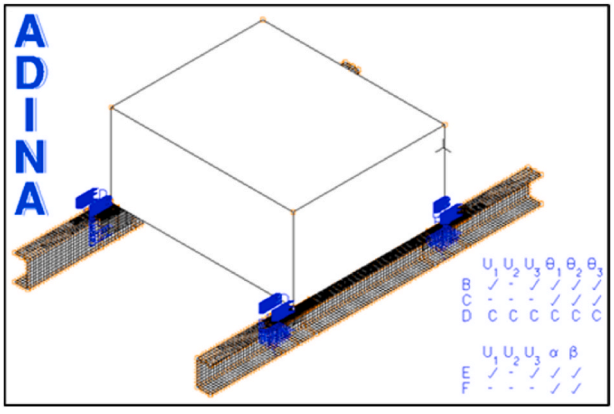

Fig. 25. FEM modal analysis: boundary condition.

Table 3
FEM modal analysis: natural frequencies and percent masses.

Mode No.	Frequency	Percent Mass (X)	Percent Mass (Y)	Percent Mass (Z)
	Hz	%	%	%
1	132.5	0.00	66.40	0.00
2	168.3	0.00	0.00	92.16
3	168.4	68.11	0.00	0.00
4	342.8	23.47	0.00	0.00
5	411.2	0.00	0.00	0.00
6	445.2	0.00	23.84	0.00
7	474.7	0.00	0.00	0.83
8	474.8	0.00	0.43	0.00
9	477.9	0.53	0.00	0.00
10	481.1	0.00	0.00	0.00
11	565.3	0.00	0.00	0.40
12	565.5	0.00	2.25	0.00
13	568.6	0.00	0.00	0.00
14	568.8	0.13	0.00	0.00
15	602.4	0.00	0.00	0.92

3.3. Dynamic analysis model

A non-linear dynamic analysis is performed using implicit Bathe Method calculation (ADINA, 2015; Bathe, 2014) starting from the static response, in which a zero-displacement function is imposed as boundary condition in the ideal points where the foundation is bolted to the shock machine.

The time step choice depends on the experimental and numerical modal analysis results, considering that, in the rigid connection case, the first natural frequencies are in the range of 150–175 Hz. To obtain a certain accuracy in the time step (Δt) selection, it has been chosen $\Delta t = 10^{-4}$, a value that corresponds to about 1/100 of natural period. In the elastic case (presence of mountings), knowing from load displacement curve (Fig. 23) the mean stiffness, it is possible to derive the natural frequency of mountings (5 Hz). The time step is selected with the same criterion of the previous case, so $\Delta t = 10^{-3}$ is chosen to achieve more accuracy. The static zero-displacement function is replaced by a displacement time history in the vertical direction (Fig. 26), which values for each test are obtained integrating twice the measured acceleration time history (Fig. 27). These measured values are considered valid until the end of the anvil table travel; then, a constant displacement is imposed to study the free response of the system. The experimental asymmetries are not corrected in reported data. Therefore, the same displacement time history measured by one accelerometer at one single structure corner is set as symmetric load input in the four model load application points. In addition, the displacement time history value can be biased due to the double integration operation.

These experimental time histories are used as load input considering their soundness to the standard time history curves conventionally used

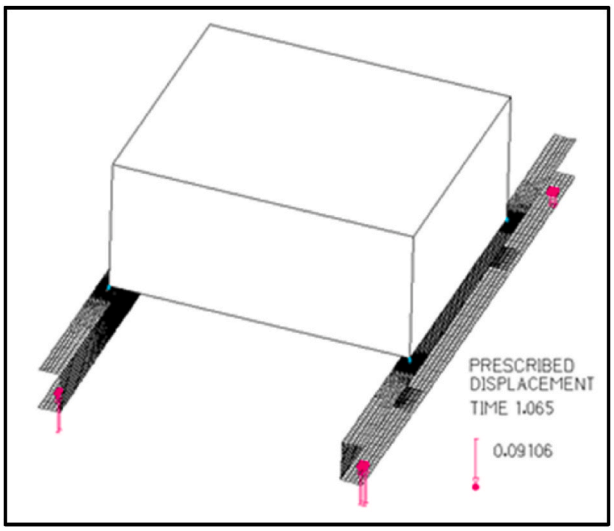

Fig. 26. Prescribed displacement vertical time history application.

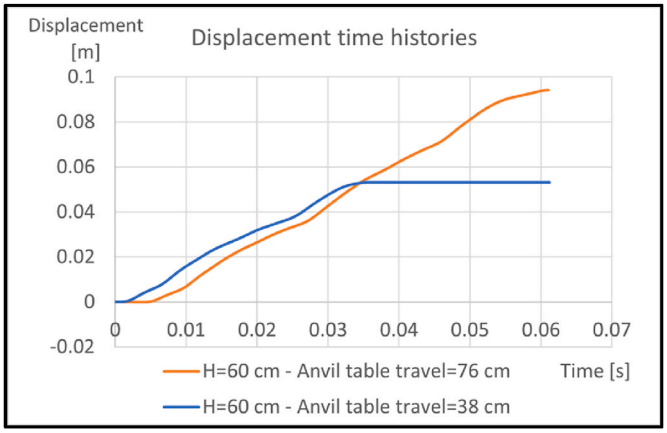

Fig. 27. Examples of displacement time histories obtained by accelerometers measurements for the rigid condition.

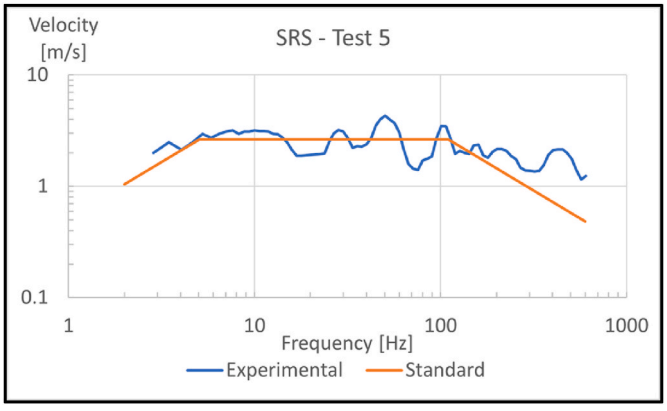

Fig. 28. Test 5 – Experimental and Standard Shock Response Spectrum comparison.

in the engineering practice. In fact, the energy input distribution is similar, as we can see in the comparison of the experimental and standard shock response spectrum (SRS): in Fig. 28, as example, the experimental SRS of tests 5, achieved from the non-filtered signal, is compared with the theoretical one. Theoretical standard SRS are

Table 4
Test 5 – Shock Response Spectrum parameters.

d_0 [m]	v_0 [m/s]	a_0 [m/s^2]
0.083	2.63	1820

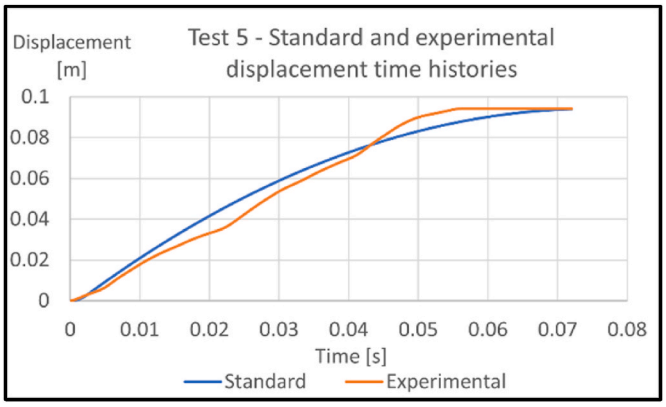

Fig. 29. Test 5 - Standard and experimental displacement time histories comparison.

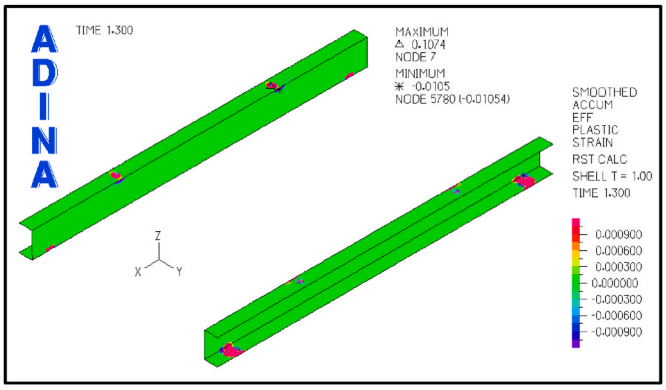

Fig. 30. Rigid connection (hammer height = 30 cm, anvil table travel = 76 mm): accumulated plastic strain.

assessed from the time history curves using the formulas reported in STANAG 4370 (2016), currently employed in design practice. As a reference, SRS parameters d_0, v_0 and a_0, obtained by the maximum displacement d, velocity v and acceleration a achieved from the experimental time histories are reported in Table 4. In Fig. 29, the related comparison of displacement time histories is reported, showing their soundness.

In a couple of cases, calculations in the dynamic analysis are run applying velocity and acceleration time histories instead of displacement ones to verify their impact on the results, without any change in the Finite Element environment.

The last time step is chosen considering 300 ms in the rigid case and 600 ms instead in the mounting condition to allow more than two free oscillations periods.

3.4. Dynamic analysis results

From dynamic analysis results it can be seen that, when the foundation is rigidly linked by bolting, the resulting strain values are high. When the hammer height is 30 cm, plastic strain is localized close to the rigid connection (Fig. 30), instead, when the hammer height increases to 60 cm, the yielding zone is extended in the neighbouring shell elements

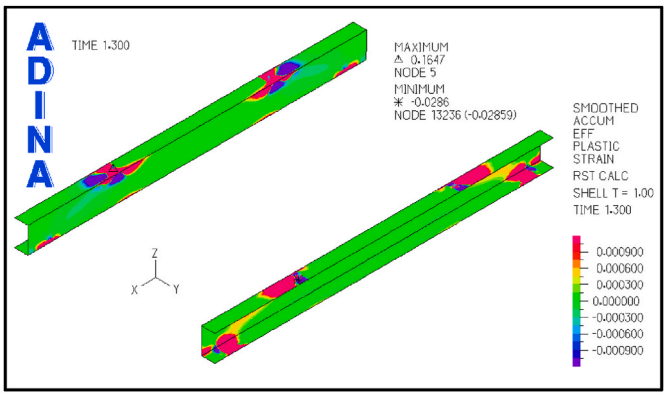

Fig. 31. Rigid connection (hammer height = 60 cm, anvil table travel = 76 mm): accumulated plastic strain.

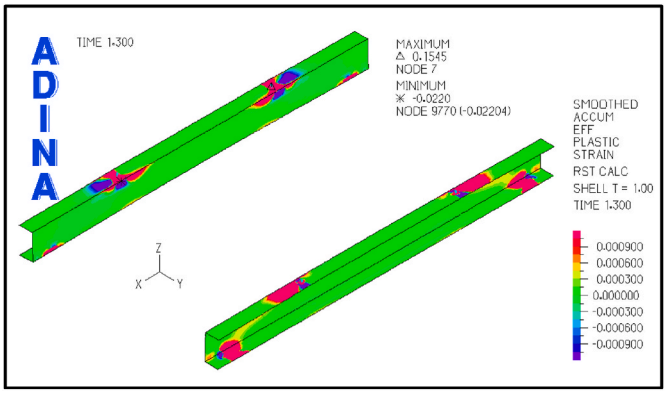

Fig. 32. Rigid connection (hammer height = 60 cm, anvil table travel = 38 mm): accumulated plastic strain.

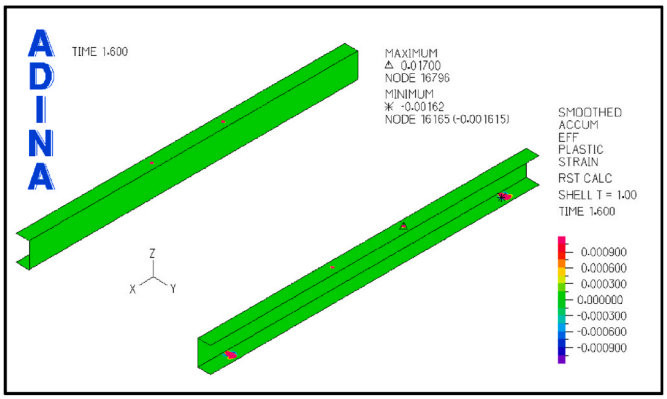

Fig. 33. Mountings connection (hammer height = 60 cm, anvil table travel = 76 mm): accumulated plastic strain.

(Figs. 31–32).

In the elastic connection case (with mountings), instead, the strain is relatively small, and no plastic strain is shown when the hammer height is 60 cm (Fig. 33) independently from the mounting simulation strategies (1, 8 and 24 connectors).

The stress concentration in the connection nodes is large as expected, due to the model approximation, so plastic strain in these elements must be neglected.

From the comparison of the numerical strains obtained applying displacement, velocity and acceleration time histories, it has been checked that a negligible impact on the results is induced by applying velocity or acceleration time histories instead of displacement ones. Therefore, results are reported for the displacement case input, without any significant change in the numerical results.

Table 5
Modal analysis: numerical and experimental comparison results.

Experimental frequency	Numerical frequency	Modal participation factor direction
Hz	Hz	Hz
152	132.5	Y-transversal
161	168.3	Z-vertical
174	168.4	X-longitudinal

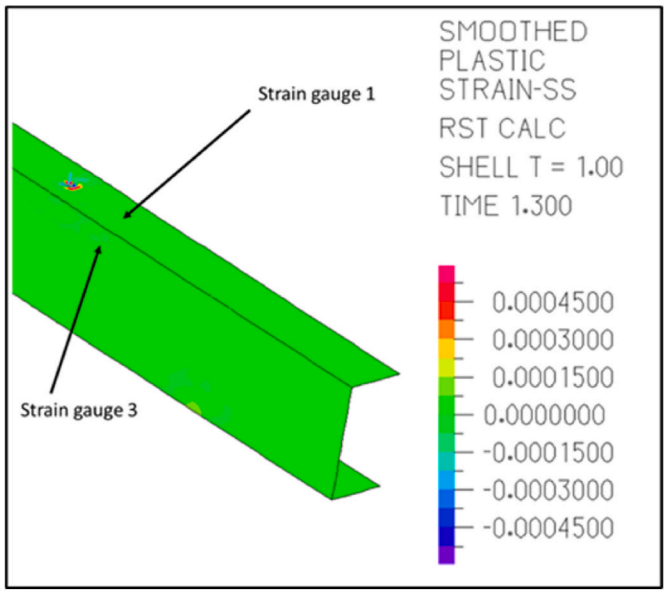

Fig. 34. Rigid connection (hammer height = 30 cm, anvil table travel = 76 mm): comparison accumulated axial plastic strain.

3.5. Experimental and numerical comparison: modal analysis

Experimental and numerical modal analysis results are compared in Table 5 showing satisfactory results. Frequency results, especially in vertical direction, are similar (4% error). This value of frequency is used to determine the time step in the dynamic implicit calculation. In fact, implicit method is unconditionally stable, but to obtain a certain accuracy the time step is determined according to the first natural frequencies of the studied structure, selecting a value of about 1/100 of natural period. This choice allows to include also high order frequencies response, considering that Bathe (2014) recommends using a value equal or less than 1/10 of the smallest natural period. Lower time step sizes are not necessary, due to the limits of the finite element methods that are not able to predict the highest frequencies response with a good accuracy (Bathe, 2014).

3.6. Experimental and numerical comparison: dynamic analysis

In dynamic analysis the FEM results are in agreement with experimental data. In the rigid case, experimentally, the shock pulse induced by the 30 cm hammer height does not produce accumulated plastic strain in the strain gauges measurements and similar results are achieved by FEM (Fig. 34). When the hammer height increases to 60 cm, strain gauges no. 1 and no. 3 shows up axial plastic strain. Similar strain levels are obtained with FEM calculation (Fig. 35). An example of comparison of strain measurements and numerical results is shown,

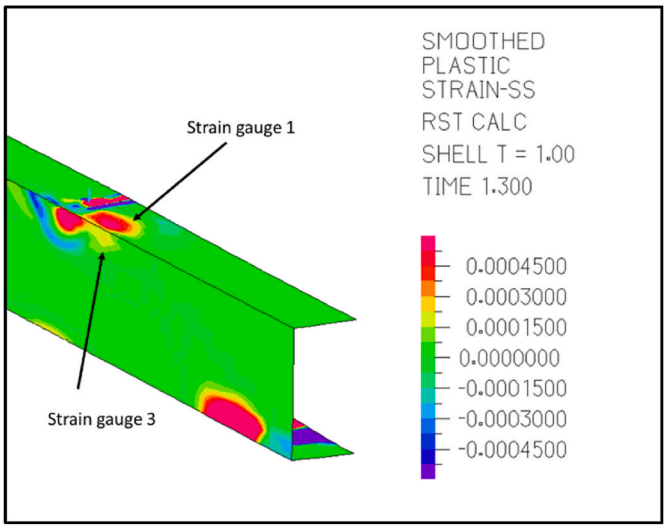

Fig. 35. Rigid connection (hammer height = 60 cm, anvil table travel = 76 mm): comparison accumulated axial plastic strain.

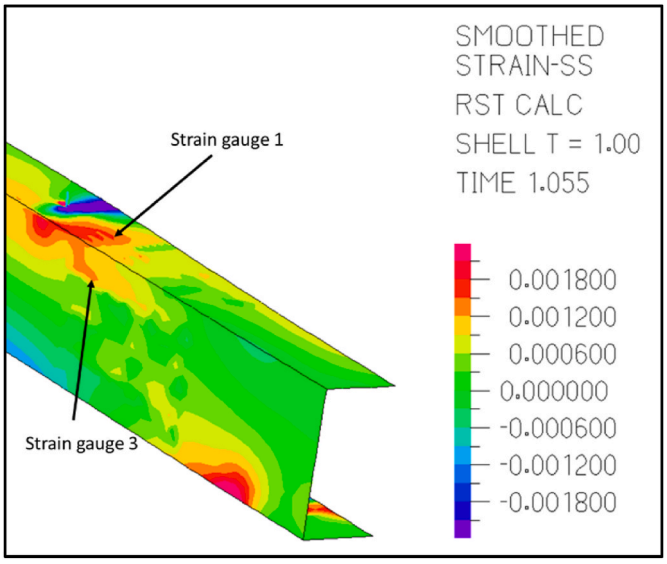

Fig. 36. Rigid connection (hammer height = 60 cm, anvil table travel = 76 mm): comparison axial strain.

considering strain gauges no 1 and 3 (most stressed ones) in the severe condition of test no. 5 in the most stressed instant of time (Fig.s 36–38, Table 6). The shear component considered is the engineering shear strain defined as $\gamma_{xy} = 2\varepsilon_{xy}$. This γ_{xy} is the angular deformation defined as the ratio between shear stress τ_{xy} and shear modulus G. In the mountings case, no yielding is found by both, measurements and calculation.

Strain numerical time histories follow the same trend of the experimental ones. Some examples are reported in Figs. 39–40 related to the rigid and the mountings connection. All the analyses provided the same trends and therefore the comparisons are limited to maximum values for the sake of shortness.

3.6.1. *Rigid connection case: comparison chart diagrams and errors table*

The numerical and experimental comparison is performed considering the absolute maximum value for each strain component in the different directions (axial, transversal and shear). In the following charts (Figs. 41-44), for each strain gauge, the strains maximum values

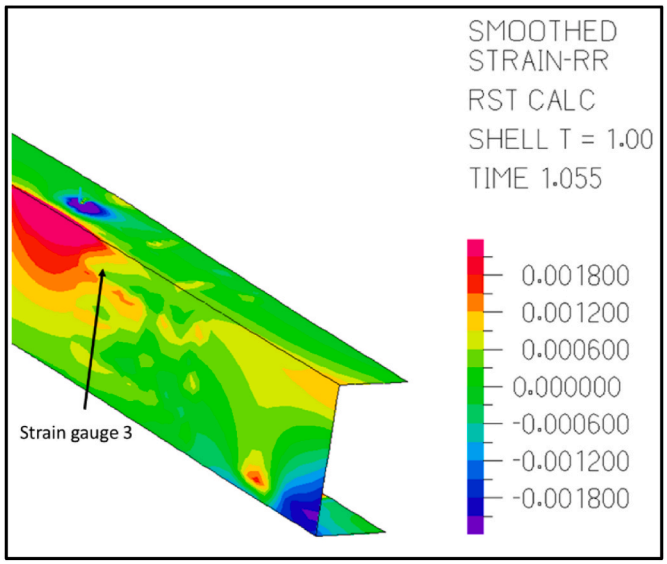

Fig. 37. Rigid connection (hammer height = 60 cm, anvil table travel = 76 mm): comparison transversal strain.

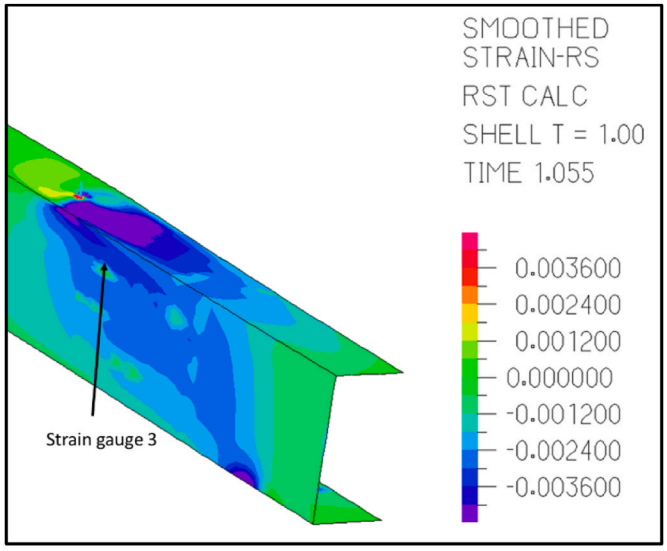

Fig. 38. Rigid connection (hammer height = 60 cm, anvil table travel = 76 mm): comparison shear strain.

Table 6
Test 5 (hammer height = 60 cm): comparison numerical and experimental strain results.

Strain gauge	Axial strain	FEM axial strain	Trasv. Strain	FEM transv. strain	Shear strain	FEM shear strain
	[10^{-3}]	[10^{-3}]	[10^{-3}]	[10^{-3}]	[10^{-3}]	[10^{-3}]
1	1.2	1.5	//	//	//	//
3	0.9	1.3	0.5	0.8	2.2	2.5

measured and the calculated ones are reported for each test. In the first diagram strains values of monoaxial strain gauges are compared with axial numerical values. Then, the strain values of rosette gages are reported in comparison with axial, transversal and shear numerical components. In tests no. 1-2-3 no input accelerometers time histories are available due to prob debonding, so only experimental strain results are

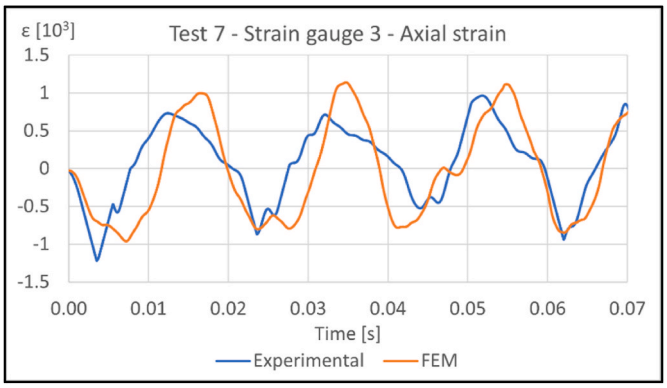

Fig. 39. Rigid connection (Test 7) - Strain gauge 3 - Axial Strain time histories comparison.

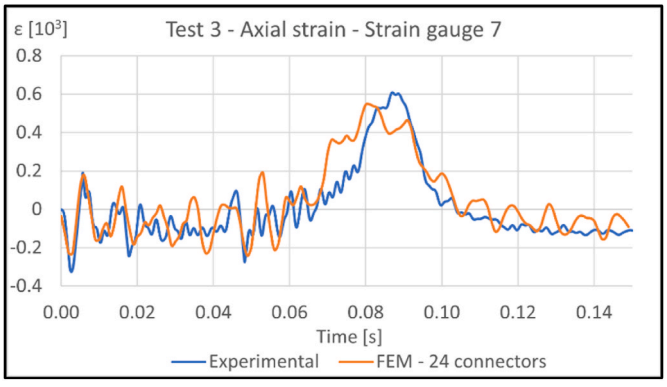

Fig. 40. Mountings connection (Test 3) - Strain gauge 7 - Axial Strain time histories comparison (24 connectors FEM model).

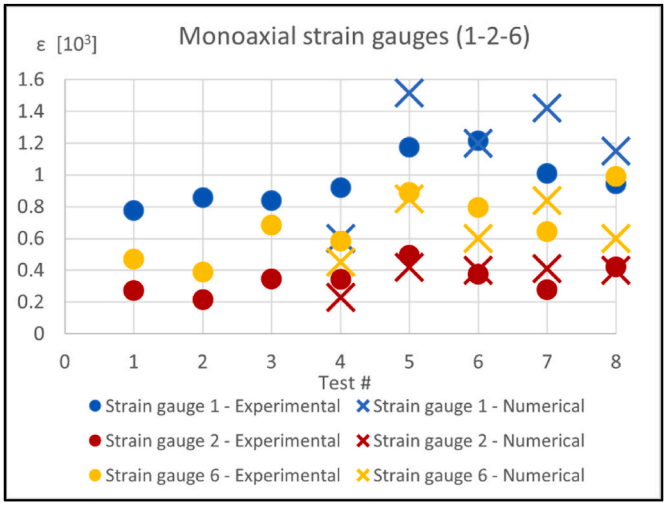

Fig. 41. Strain gauge no. 1-2-6: axial strain comparison.

shown. The average percentage error considering all tests data with respect to the FEM results for each strain component is shown in Table 7.

While axial and transversal strain components are satisfactorily simulated and show good agreement with test results, the shear is rather biased. This can be due to the model approximation in the simulation of the load inputs. In fact, the more relevant error occurs in the low part of the beams (strain gauge 4 and 5), close to the load application elements. The displacement time histories are set in the ideal points where the

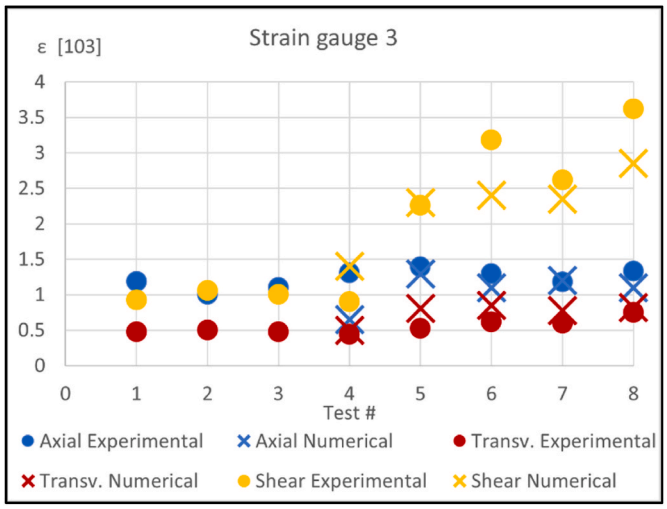

Fig. 42. Strain gauge no. 3: strain comparison.

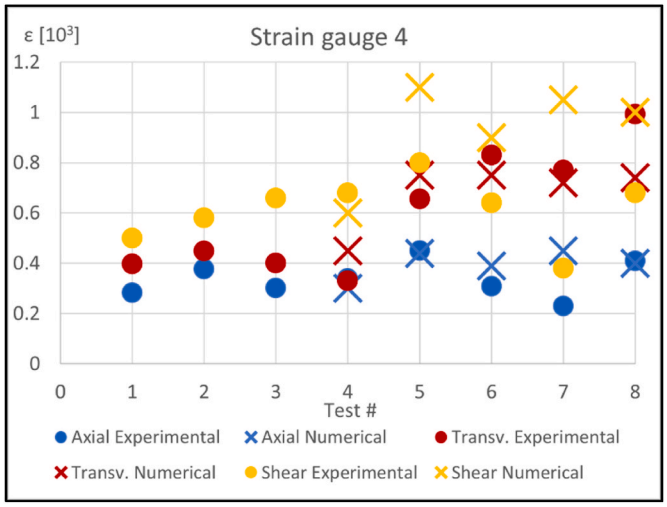

Fig. 43. Strain gauge no. 4: strain comparison.

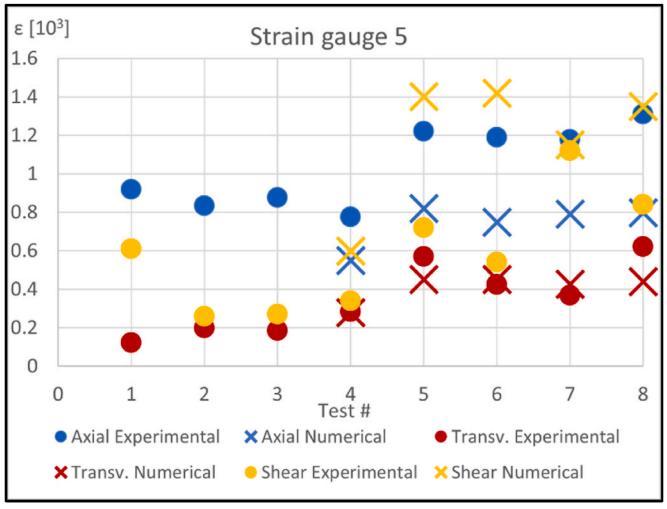

Fig. 44. Strain gauge no. 5: strain comparison.

Table 7
Rigid connection case: percentage errors for strain component of the numerical method.

Axial	Transversal	Shear
%	%	%
−5.2	8.2	45.9

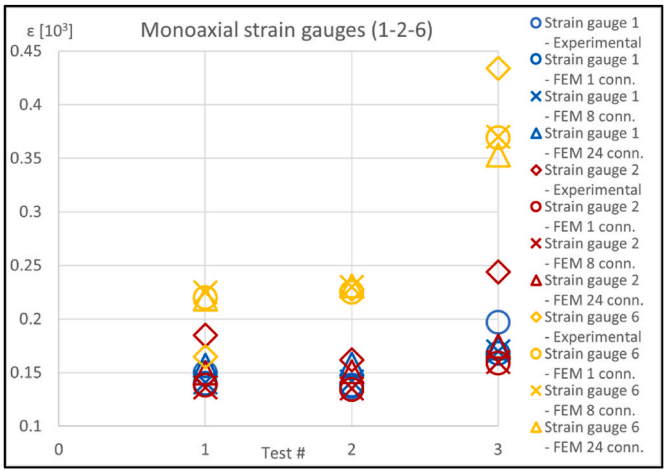

Fig. 45. Strain gauge no. 1-2-6: axial strain comparison.

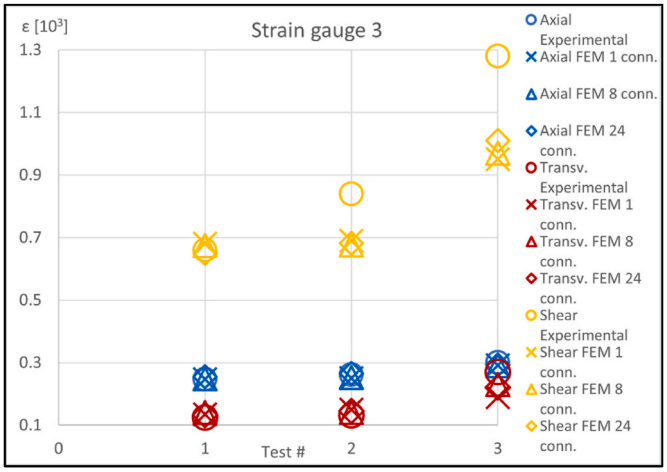

Fig. 46. Strain gauge no. 3: strain comparison.

foundation is bolted to the shock machine, but the contact non-linearities are neglected. It is also worth noting that measurements were taken in one position only and mirrored on the others three supports, assuming double symmetry of the problem. Therefore, asymmetrical effect likely occurring during tests could not be accounted for.

3.6.2. Mountings connection case: comparison chart diagrams and errors table

The comparison is shown using chart diagrams (fig.s 45–49) as in the previous section. However, three different mounting modeling strategies have been proposed. Results are presented considering all of them, i.e. using 1, 8 and 24 link connectors to better account for longitudinal and transversal dynamic effects and interactions. The shear strain values of strain gauges nr. 5 are missing because these data are corrupted. The average percentage errors are also provided with reference to the different mounting (see Table 8).

The experimental vs. numerical comparison is again rather

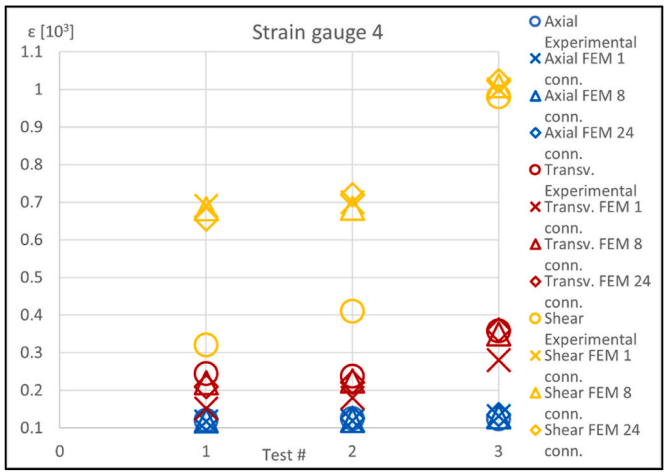

Fig. 47. Strain gauge no. 4: strain comparison.

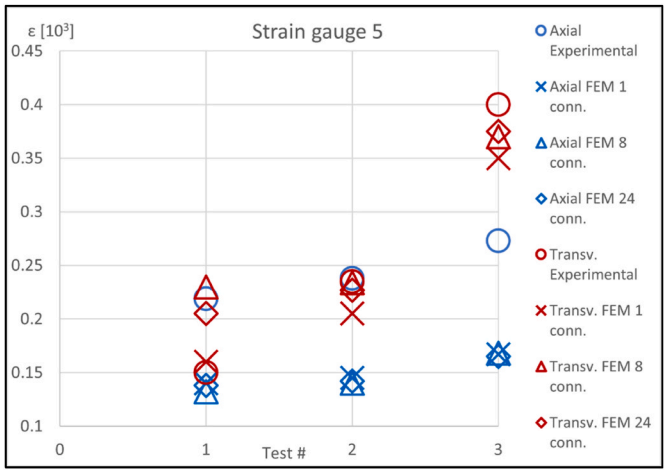

Fig. 48. Strain gauge no. 5: strain comparison.

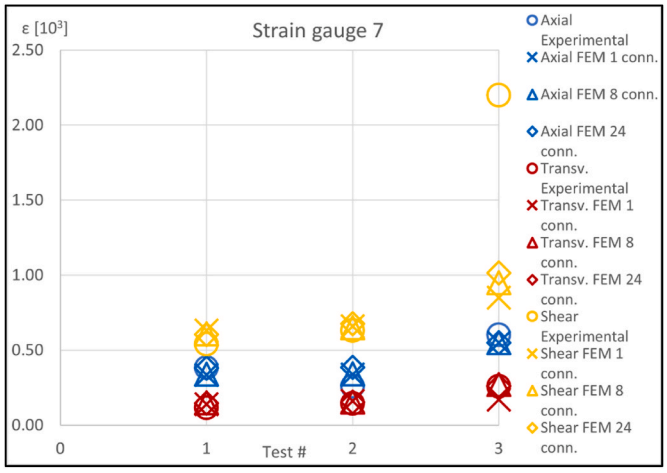

Fig. 49. Strain gauge no. 7: strain comparison.

satisfactory and the enhanced simulation model contribute to reduce the bias up to very good agreement. Shear strain component is still deviating but less than the rigid connection case. It appears that mounting modeling strategy has no influence on the shear behavior.

Table 8
Mountings connection case: percentage errors for strain component of different numerical mountings models.

Axial 1 connector	Axial 8 connectors	Axial 24 connectors	Transv. 1 connector	Transv. 8 connectors	Transv. 24 connectors	Shear 1 connector	Shear 8 connectors	Shear 24 connectors
%	%	%	%	%	%	%	%	%
−9.9	−9.5	−5.1	−9.5	6.0	3.3	16.3	16.0	17.2

4. Conclusions

The comparison between non-linear dynamic implicit calculations and test results obtained according to MIL S 901 D standard resulted rather satisfactory. Some reliable guidelines of shock foundation design in dynamic calculation have been provided. A very fine mesh patterns as suggested by classification societies' rules is used providing results in good agreement with experimental data, while time step should be determined according to the natural frequencies of the studied structure. No significative differences in the results are shown, applying displacement, velocity or acceleration time histories as load input. The choice to propose different mounting models in the FE method has led to a better accuracy when the mounting simulation is more realistic (8 or 24 connectors), especially in the axial and the transversal strain component comparison (see Table 8). However, it is believed that dynamical characterization of materials is crucial and, before starting time-consuming calculations, it is worth obtaining a comprehensive dataset to feed the finite element models as such input data largely affect the numerical results.

Stress concentration effect is intrinsic in the numerical structural model at sharp notches. According to well-known theory of continuum mechanics, stresses at sharp notch tip tends toward infinite. Of course, in reality plasticization of material occurs and a micro-supporting effect in way of notch tip is postulated after Neuber. Such effect can only be avoided using conventional geometries (i.e. fictitious notch rounding) or conventional stress extrapolations (Radaj and Vormwald, 2013). Therefore, in the engineering practice these numerical values, shown in the FE results in the connection nodes, must be neglected.

While the work presented in this paper is referring to a specific and simplified foundation structure of onboard machinery items, the implemented FEM procedure could be applied to similar geometries and lay-out configurations of hull structures provided that an appropriate displacement time history at selected points is available as a loading condition. The input loads used in the present work and derived by rule requirements proved to be sound and effective. Even if calculations are run applying experimental time histories as load input, the implemented FEM procedure can also be considered valid using standard displacement time history loads conventionally used in the engineering practice as it demonstrated their soundness.

Further tests are planned in the next months to improve numerical model settings and to study structural response of other materials, namely of marine composites. The most relevant differences between calculation and experiments occur for the shear strain component and require further investigation about their origin. A hypothesis could be related to the non-linearities that it wasn't possible to account for in this work (contact phenomenon, asymmetries, etc …), but that could be analyzed in future investigation, using enhanced strain measurements techniques.

CRediT authorship contribution statement

F. Mannacio: Conceptualization, Methodology, Software, Validation, Formal analysis, Investigation, Writing, Visualization. **A. Barbato:** Conceptualization, Methodology, Resources, Supervision, Writing. **F. Di Marzo:** Conceptualization, Methodology, Resources, Data curation, Investigation, Writing. **M. Gaiotti:** Conceptualization, Methodology, Resources, Writing. **C.M. Rizzo:** Conceptualization, Methodology, Resources, Supervision, Writing. **M. Venturini:** Conceptualization, Methodology, Resources, Data curation, Investigation, Writing.

Declaration of competing interest

The authors declare that they have no known competing financial interests or personal relationships that could have appeared to influence the work reported in this paper.

Acknowledgements

This work has been possible with the help of Brondi srl La Spezia, which has provided materials and equipment to prepare the tests. We also acknowledge the qualified personnel in Naval Experimentation and Support Centre (CSSN) of La Spezia, in particular Mr. Vincenzo Accardi, who contributed to the phases of setting, performing and post processing of tests.

References

ADINA, 2015. Theory and Modeling Guide Volume I. Watertown. ADINA R & D, Inc.
Bathe, K.J., 2014. Finite Element Procedures. Watertown, Bathe, K.J.
Clements, E.W., 1972. Shipboard Shock and Navy Devices for its Simulation. Naval Research Laboratory, Washington, D.C.
Coats, T., et al., 2003. Component Representation for Shock Qualified Foundation Structure, Shock and Vibration, vol. 10. IOS Press, pp. 71–80.
Ewins, D.J., 2000. Modal Testing: Theory, Practice and Application. Research Studies Press LTD, Hertfordshire.
HIPEBA, 2015. Criteria for Selection of High Performance Steel Properties and Processes Definition Complementary Report Deliverable d.2.1 and Deliverable 2.2.
Mannacio, F., et al., 2021. Analysis of the Underwater Explosion Shock Effects on a Typical Naval Ship Foundation Structure: Experimental and Numerical Investigation, MARSTRUCT 2021 Congress, Trondheim, pp. 7–9. June 2021.
ME'scope VES, 2014. Tutorial Manual Volume IA. Scotts Valley. Vibrant Technology, Inc.
MIL-S-901-D, 1989. Shock Tests, h.I. (High-impact) Shipboard Machinery, Equipment, and Systems, Requirements. United States Department of Defense.
NAV-30-A001, 1986. Norme per l'esecuzione delle prove d'urto su macchinari ed apparecchiature di bordo, Ministero della Difesa. Istituto Poligrafico dello Stato.
NAVSEA 0908-LP-000-3010, Rev. 1, 1995. Shock Design Criteria for Surface Ships, Naval Sea Systems Command.
O'Hara, G.J., Belsheim, R.O., 1963. Interim Design Values for Shock Design of Shipboard Equipment. US Naval Research Laboratory, Washington D.C.
Powerflex, 2010. PWHS series helical standard Technical data & performance characteristics. Limatola: Powerflex Srl. https://docplayer.net/43762263-Powerflex-pwhs-series-powerflex-pwhs-series-stainless-steel-cable-dampers-are-designed-to-preform-efficiently-without-material-or-performance-degrad.html.
Radaj, D., Vormwald, M., 2013. Advanced Methods of Fatigue Assessment. Springer.
Remmers, G.M., O'Hara, G.J., Cuniff, P.F., 1996. Review Dynamic Design Analysis Method DDAM, Shock and Vibration, vol. 3. John Wiley & Sons, Inc, p. 461, 176.
Scavuzzo, R.J., Pusey, H.C., 2002. Naval Shock Analysis and Design, the Shock and Vibration Analysis Center. HI-TEST Laboratories, Inc.
SMM/CN 300 DVD, 1978. Criteri e metodi per il proporzionamento e la qualificazione antiurto dei componenti destinati alle Unità navali. Stato Maggiore Marina, Istituto Poligrafico dello Stato.
STANAG 4141, 1976. Shock Testing of Equipment for Surface Ships. NATO Standardization Agreement.
STANAG 4370, 2016. Environmental Testing - AECTP-100 – 600. NATO Standardization Agreement.